Atomic-scale structure and work function of the K-adsorbed Pd(110)-(1 × 2) surface

Kazuyuki Higashiyama[1,2]* and Akihiro Egami[1]†

[1]*Graduate School of Pure and Applied Sciences, University of Tsukuba, Tsukuba 305-8571, Japan*
[2]*Faculty of Pure and Applied Sciences, University of Tsukuba, Tsukuba 305-8571, Japan*

The (110) surface of Pd shows a (1 × 2) symmetry when a small amount of K is adsorbed. The structure of this (1 × 2) surface is studied by scanning tunneling microscopy (STM), work function measurement and ab initio density functional theory. Atom-resolved STM images confirm the missing-row reconstruction of the Pd substrate; the K atoms are invisible at coverage of 0.1 monolayer, while they appear as bright rows at 0.3 monolayer. The work functions are calculated for a model in which K atoms are arranged along the grooves of the reconstructed Pd substrate. The calculation agrees very well with the experiment. According to the theory by Tersoff and Hamann, the STM images are analyzed in terms of the local density of states at the Fermi level. The analysis explains why the K atoms become visible with an increase in coverage.

1. Introduction

Alkali metals are important materials for fundamental research and industrial applications. One of the topics in surface science is the alkali-metal-induced surface reconstruction. Especially, the (110) surfaces of fcc transition metals are interesting because many of the surfaces show a (1 × 2) symmetry with the presence of alkali metals.[1)] The structure of this (1 × 2) surface has been studied by various techniques. The list includes low-energy electron diffraction (LEED),[2–4)] scanning tunneling microscopy (STM),[5–9)] ion scattering[10–12)] and X-ray standing waves.[13)] Most of the studies support the missing-row model[14)] in which every second atomic row in the topmost layer of the substrate surface is removed.

In contrast, the structure of adsorbed alkali metals is not well-established. This situation is mainly due to the absence of long-range order in the alkali adlayers, as evidenced by the presence of streaks in the LEED patterns. Typical examples are Na, K and Cs on Ni(110). Gerlach and Rhodin[15,16)] analyzed these streaks and proposed an out-of-phase arrangement of the alkali-atom rows (hereafter, alkali rows) on an unreconstructed Ni(110) surface. Behm

†Present address: CANON ANELVA CORP., Kawasaki 215-8550, Japan
*E-mail:higashiyama.kazuy.ka@u.tsukuba.ac.jp

et al.[17] refined this alkali-row model by taking into account the missing-row reconstruction of the Ni(110) surface. In the model, the alkali rows were assumed to be located in the grooves between the first-layer Ni rows. An effective-medium-theory study on K/Cu(110)[18] supported the alkali-row model. Scanning-tunneling-microscopy studies were reported for K/Cu(110),[5,6] Cs/Cu(110),[6,7] K/Rh(110),[8] K/Ag(110),[9] and K/Au(110).[6,9] In these studies, however, alkali atoms adsorbed on the (1×2) surface were invisible or appeared as hollows in the STM images. Further detailed investigation is needed to confirm the model.

The K-adsorbed Pd(110) surface is known to show a (1 × 2) LEED pattern at coverage of 0.095 monolayer (ML).[19] Here we report on a study of the K-adsorbed (1×2) surface by using STM, work function measurement and ab initio density functional theory. Our study gives strong support to the alkali-row model. The paper is organized as follows. Section 2 describes the experimental and computational methods. In Sect. 3, a structural model compatible with the alkali-row model is proposed on the basis of the ab initio calculations. In Sect. 4, the experimental results are presented and compared with the calculations. The effects of local density of states on the STM images are discussed.

2. Methods

2.1 Experimental

An ultrahigh-vacuum apparatus for STM and LEED has already been described.[20] The apparatus was also equipped with a facility for X-ray photoelectron spectroscopy. It consisted of a twin-anode X-ray tube and an electron energy analyzer. The analyzer and a LEED gun were used for measuring electron-energy loss spectra. A mirror-polished Pd(110) sample with 99.999% purity was cleaned by cycles of argon ion sputtering and annealing at 500°C. The cleaned surface showed no contaminations in the photoelectron spectra and displayed a sharp (1 × 1) LEED pattern with low background. Potassium exposure was made via a commercial getter source at a rate of 0.023 ML/min (1 ML is the surface atomic density of a truncated Pd(110) surface). The estimation of K coverage θ (in ML) is described in Appendix. The pressures during K exposure were below 1×10^{-8} Pa. Potassium-covered Pd(110) surfaces displayed a series of LEED patterns with an increase in θ: (1×1) → (1×3) → (1×2) → (1×2) + streaks. Some of the LEED patterns are shown in Fig. 1. A well-ordered (1 × 2) surface was obtained by depositing 0.5-ML K onto a clean (1 × 1) surface at room temperature followed by annealing at 500°C. The (1 × 2) surfaces at higher θs were made by depositing K onto a room-temperature (1 × 2) surface. The coverage dependence of streaks in the LEED pattern was similar to those reported for the other alkali-covered fcc (110) surfaces.[15–17] The

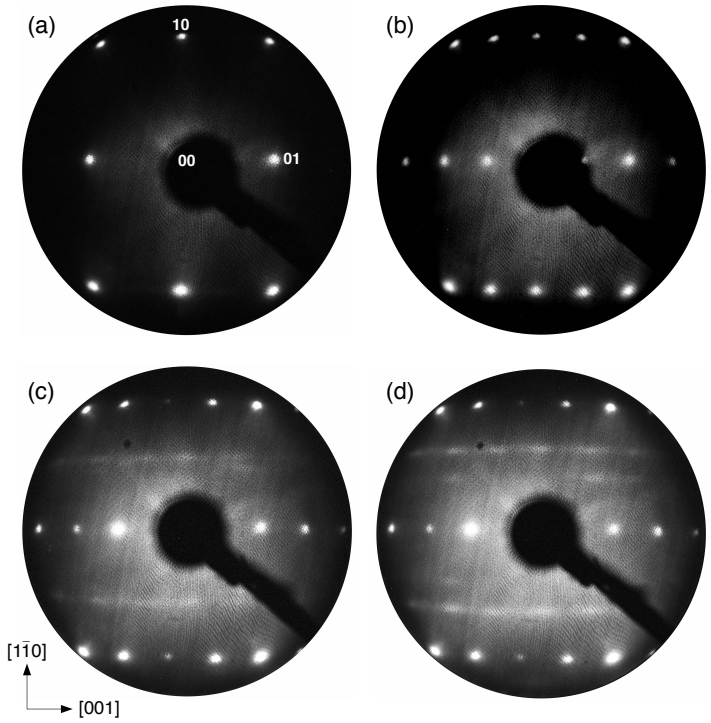

Fig. 1. LEED patterns of clean and K-covered Pd(110) surfaces: (a) clean; (b) (1 × 2), 0.1 ML; (c) (1 × 2) + streaks, 0.23 ML; (d) (1 × 2) + streaks, 0.3 ML. Beam energy is 78 eV.

STM observation was performed only for a freshly prepared surface because the irradiation with X-rays and electrons seriously degraded the images. The images were acquired in the constant-current mode with the bias voltage applied to the sample. The work function change with θ was measured from the shift of a low-energy cutoff in the electron-energy loss spectra. After a course of the measurements, a clean (1 × 1) surface was restored by extended cycles of sputtering and annealing.

2.2 Computational

Ab initio calculations were performed by using the Quantum ESPRESSO package[21] and the projector-augmented-wave potentials.[22] The Perdew-Burke-Ernzerhof[23,24] exchange-correlation functional was employed within the generalized gradient approximation. Plane waves were expanded up to an energy of 544 eV. The lattice constant a of bulk Pd was determined by evaluating the total energy E_{tot} as a function of a, and by fitting the Birch-Murnaghan equation of state to $E_{\mathrm{tot}}(a)$. This procedure yielded $a = 3.94881$ Å. The lattice constant thus derived was used throughout this study.

Periodic slabs separated by vacuum were used to simulate the K-adsorbed Pd(110) surface. The slab consisted of nine Pd layers and two K layers on both surfaces, and the thickness

of vacuum was 15 Å. Before performing the self-consistent calculations, all the atoms in the slab, except for the center-layer Pd atoms, were relaxed according to the standard optimization procedure. After the structure optimization, the forces acting on the atoms were below 0.026 eV/Å. Self-consistent (density-of-states) calculations were made by using the uniform k points[25] of $6 \times 4 \times 1$ ($18 \times 12 \times 1$). The Methfessel-Paxton[26] smearing with a width of 0.13 eV was employed for Brillouin-zone integrations. The work function was calculated by using the following expression,

$$\Phi = V - E_{\mathrm{F}}, \tag{1}$$

where Φ is the work function, V the electrostatic part of the total potential (excluding the exchange-correlation potential), and E_{F} the Fermi level. The potential V was evaluated by averaging over 100×100 points in the unit cell at the midpoint of vacuum. This method yielded $\Phi = 4.88$ eV for the Pd(110)-(1×1) surface, which agrees with that reported in the earlier study.[27] It should be noted that asymmetric slabs with a single K layer produced the erroneous work functions because of the presence of electric fields due to the surface dipole layers.[28] Good convergence was obtained with respect to the cutoff energy, k-point density, and slab and vacuum thicknesses.

3. Model

A particular feature of the alkali-row model is the absence of long-range order in the direction perpendicular to the rows.[15–17] Figure 2(a) illustrates an original K-row model at $\theta = 1/4$. Although K atoms in each row are regularly arranged at a distance of $2b$ ($b = \sqrt{2}a/2$), the sequence of these rows along the [001] direction is irregular. The surface depicted in Fig. 2(a) produces a (1×2) diffraction pattern with streaks located halfway between the (00) and (10) spots. The model consists of two closely related structures; one is the (2×2) structure as shown in Fig. 2(b), and the other is the c(2×4) structure in Fig. 2(c). An important difference between the two structures is the sequence of K rows in the [001] direction: AAAA... or BBBB... for (2×2), but ABAB... for c(2×4). The total energies of the two structures, however, were found to be equal within the uncertainty of 1 meV. This means that the K rows favor both A- and B-types as the neighboring rows. We thus propose a structural model of AAAA type for this system because the periodic boundary condition makes the calculations more tractable.

Figure 3 shows the K-row model used in our study. For $\theta = 1/12$ and $\theta = 1/4$, K adsorption to the hollow sites in the second Pd layer is assumed. This is because the total energy for the hollow site is lower than that for the bridge site; the energy difference per atom is 43

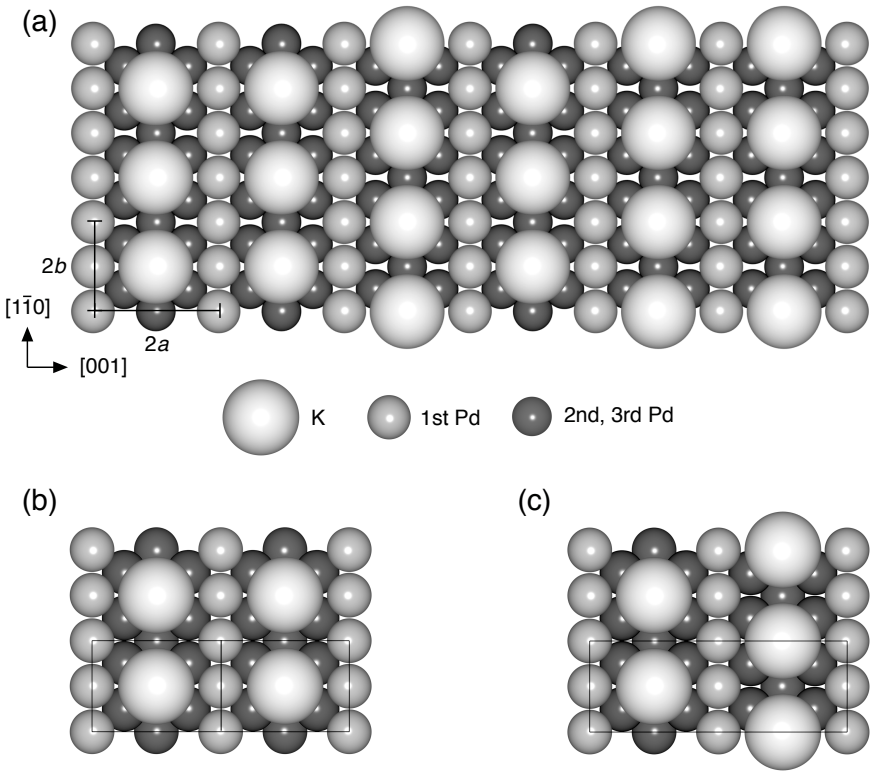

Fig. 2. Top view of a hard-spheres representation[29] of (a) original K-row model at $\theta = 1/4$, (b) (2×2), and (c) c(2×4) structures. Solid lines denote the unit cells.

(51) meV at $\theta = 1/12(1/4)$. The dimerization of K atoms is unfavorable because the structure optimization made the K dimer dissociated into two separate K atoms. Instead, the dissociated K atoms were adsorbed to the hollow sites separated by $2b$. The similar dissociation and adsorption was observed for the K trimer. These calculations imply local ordering of K atoms with a distance of $2b$ in the coverage range $1/12 < \theta < 1/4$. The complete K rows will be formed at $\theta = 1/4$, as shown in Fig. 3(b). Above 1/4 ML, the nearest-neighbor distance of K rows will decrease with an increase in θ[15,16] and reach a minimum of $3b/2$ at $\theta = 1/3$. This scenario is consistent with the coverage dependence of streaks in the LEED pattern (see Fig. A·2). For the surface at $\theta = 1/2$, we adopted the model similar to that used in Ref. 18. The LEED patterns observed at $\theta > 1/3$ displayed high background intensity. This indicates the presence of some disorder. Therefore, the model shown in Fig. 3(d) should be a tentative one. For the models except for Fig. 3, the (4×2) or (5×2) unit cell was used. The optimized coordinates of all the models used in this study are given in the supplementary data.

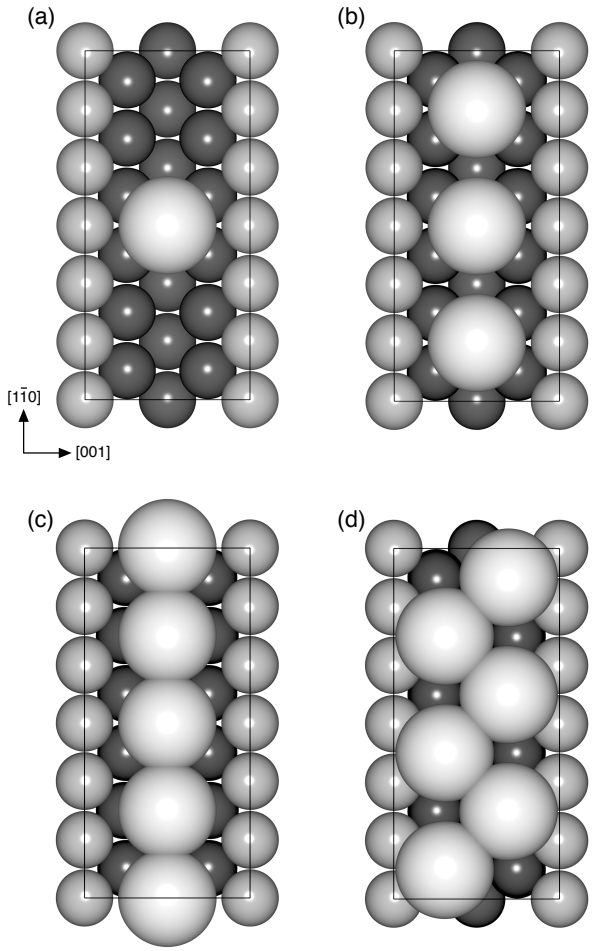

Fig. 3. Same as in Fig. 2, but for the K-row model used in this study: (a) 1/12 ML; (b) 1/4 ML; (c) 1/3 ML; (d) 1/2 ML. Solid lines indicate the (6×2) unit cell.

4. Results and discussion

4.1 Work function measurement and the comparison with theory

It is well known that the work function is sensitive to the atomic structures and electronic states of solid surfaces.[1,27,30] Figure 4 shows variation of the work function measured for the K-adsorbed (1×2) surface as a function of coverage (filled black squares). The data is expressed in the form of the work function change $\Delta\Phi$ with respect to the work function of the clean surface (5.13 eV in experiment[31] and 4.88 eV in theory). The experimental work function decreased with an increase in coverage, and reached a value close to that of polycrystalline K (2.29 eV)[32] at around 0.6 ML. A maximum of $\Delta\Phi$ is 2.81 eV, which is comparable to those reported for the K-adsorbed metal surfaces.[1] The so-called work function minimum was not observed in this system.

The work function changes calculated for the K-row model shown in Fig. 3 and the others

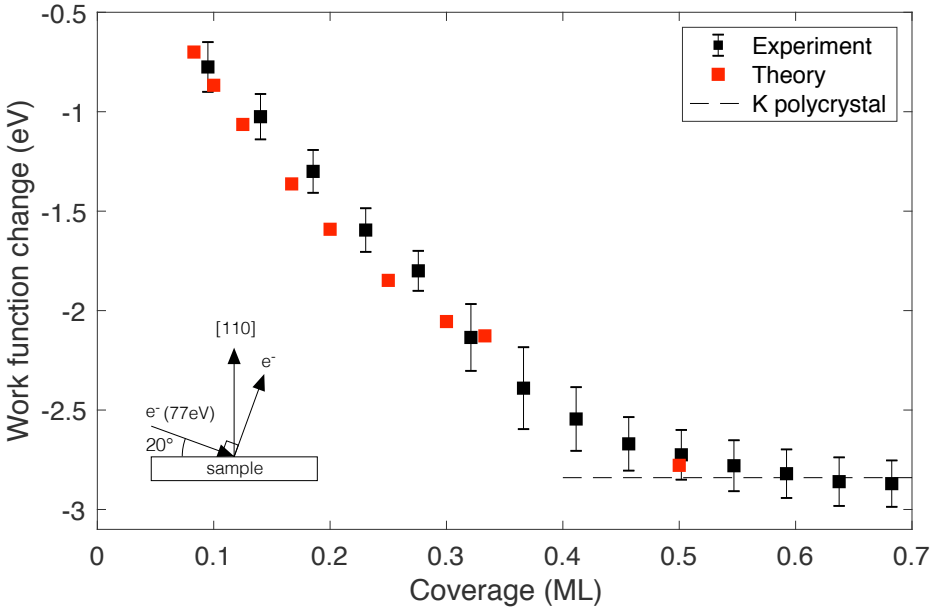

Fig. 4. Plot of the work function changes measured for the K-covered (1×2) surface (solid black squares) and those calculated for the K-row model (solid red squares). The inset shows an experimental geometry for work function measurement.

Table I. Work function changes calculated for K-adsorbed (1×2) and (1×1) surfaces.

Coverage (ML)	1/12	1/6	1/4	1/3	1/2
Calculation					
$\Delta\Phi(1 \times 2)$ (eV)	-0.70	-1.36	-1.85	-2.13	-2.78
$\Delta\Phi(1 \times 1)$ (eV)	-1.08	-1.94	-2.53	-2.81	-2.82

are plotted in Fig. 4 (filled red squares). The calculation agrees very well with the experiment. On the other hand, the adsorption to the (1×1) surface produced $\Delta\Phi$s that disagree with the experiment (see Table I). The work function of the clean surface differs by 0.25 eV between the experiment and theory. The quantum size effect[33,34] due to a finite slab thickness was evaluated to be 0.03 eV. The combined uncertainty in the calculation is 0.04 eV, which is too small to account for the 0.25-eV difference. Although the reason for this discrepancy is unknown, the agreement shown in Fig. 4 confirms that the K-row model is applicable to this system.

4.2 STM observation and the comparison with theory

Atom-resolved STM images taken for clean and K-adsorbed Pd(110) surfaces are shown in Fig. 5. In the clean surface, Pd atoms appear as bright protrusions and form a (1×1) rectangular

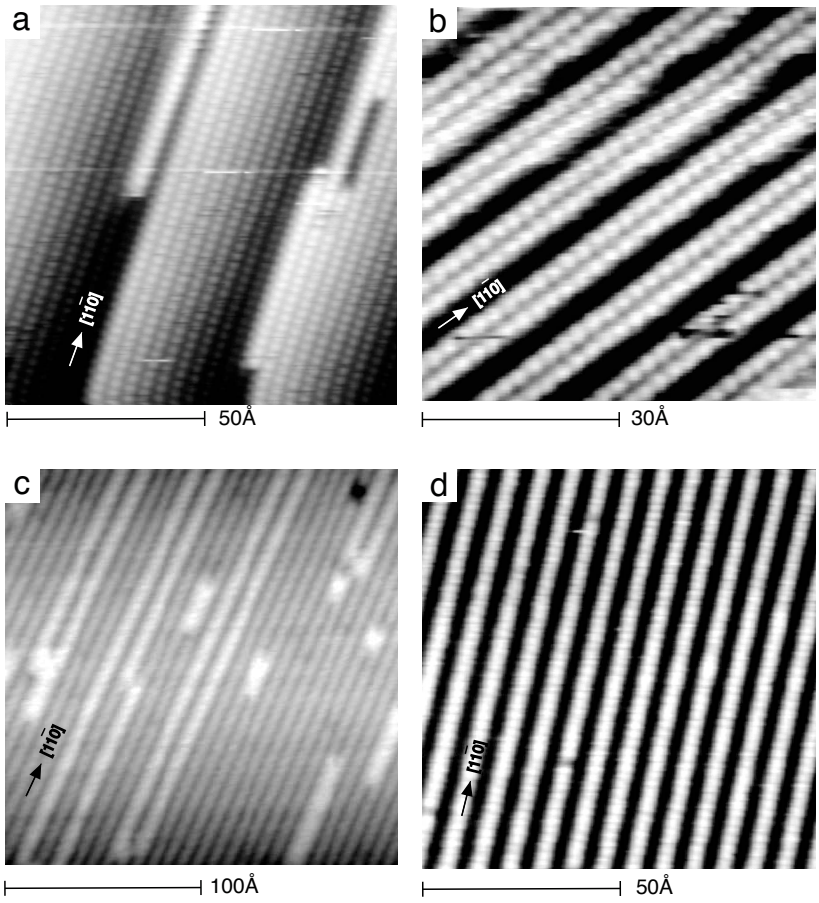

Fig. 5. STM images of clean and K-covered Pd(110) surfaces: (a) clean (-0.5 mV, 2.2 nA); (b) (1×3) (-0.5 mV, 3.2 nA); (c) (1×3) + (1×2) (-17 mV, 0.47 nA); (d) (1×2) (-4 mV, 8.4 nA). Bias voltage and tunneling current are given in brackets. Coverage of (d) is 0.1 ML.

lattice. Its lattice parameters accord with the crystallographic data. The corrugation amplitude is approximately 0.2 (0.4) Å along the [1$\bar{1}$0] ([001]) direction. The (1×3) structure is of the missing-row type with every third atomic row missing. In most cases, the (1×3) structure was observed in the form of patches and coexisted with either the (1×1) or (1×2) phase as indicated in Fig. 5(c). The (1×2) structure is also of the missing-row type. The corrugation amplitude in the [001] direction is about 0.5 Å. The (1×2) structure was well ordered and extended over the terraces with typical sizes of several hundreds of angstroms. No K atoms were observed in the coverage range $\theta \leq 0.1$.

Figure 6 shows STM images taken for the (1×2) surface at $\theta = 0.3$. Most part of the terraces are covered with a different type of rows. In addition, these rows are located in the grooves created by the missing-row reconstruction. We attribute these bright rows to K rows formed in the grooves between the first-layer Pd rows. The similar bright rows were reported

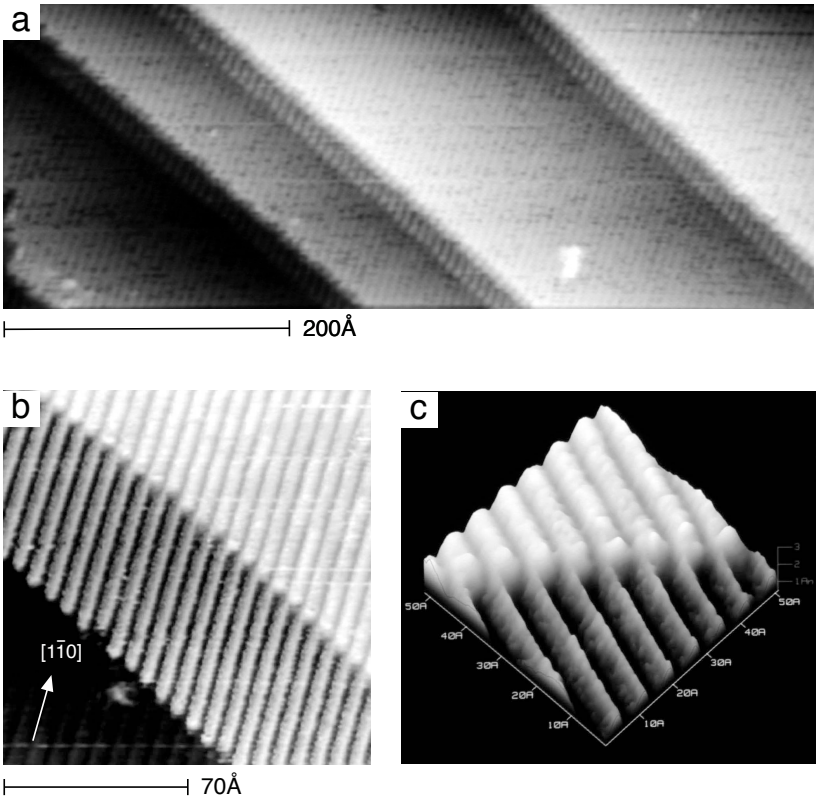

Fig. 6. STM images of the (1×2) surface at $\theta = 0.3$. Bias voltage and tunneling current are (a) -0.5 mV, 1.0 nA, and (b) -4 mV, 1.0 nA. Three-dimensional view of (b) is shown in (c).

for the Cs/Cu(110)-(1×3)[35] and K/Ag(110)-(1×1)[9] surfaces. The corrugation amplitude along the [001] direction is about 1.0 Å. The images in Figs. 5 and 6 were obtained only when the bias voltages were low. The use of high bias voltages resulted in very unstable tunneling or crashes of the tip to the sample surface. The voltage polarity had no significant effect on the images. These observations suggest that electrons near E_{F} participate in the tunneling. For $\theta > 0.3$, no high-quality images were obtained.

According to the theory of STM,[36] the tunneling current is proportional to the local density of states (LDOS) of a sample surface. Since the constant tunneling currents are used in our experiment, the STM images thus obtained can be interpreted in terms of the constant LDOS surfaces. Figures 7(a)–7(c) show contour plots of LDOSs at E_{F} calculated for the model shown in Figs. 3(a)–3(c). The distribution of LDOSs above the K atoms changes considerably with coverage θ; contour lines show hollows at $\theta = 1/12$, while they display protrusions at $\theta = 1/3$. This coverage dependence of the contour lines is consistent with the STM images shown in Figs. 5(d) and 6(b). The appearance of protrusions in Fig. 7(c) means that the K LDOS at $\theta = 1/3$ is higher than that at $\theta = 1/12$. Figure 7(d) indicates that the high K LDOS

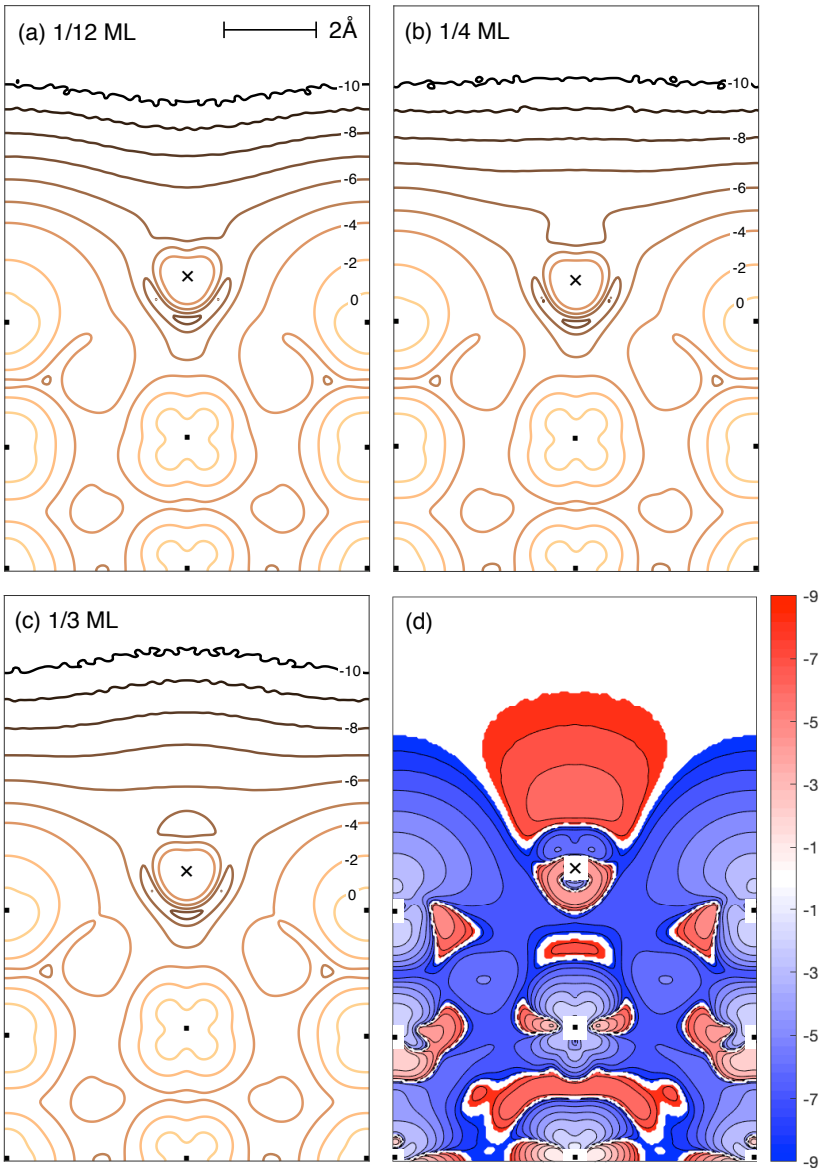

Fig. 7. Logarithmic plots of LDOSs at E_F calculated for the K-row model: (a) 1/12 ML; (b) 1/4 ML; (c) 1/3 ML. The unit of LDOS is the number of states per (a.u.)^3 (1 a.u. = 0.529 Å), per Ry (1 Ry = 13.606 eV). Shown is a $(1\bar{1}0)$ plane containing K (crosses), and Pd (solid squares) in the first, third, and fifth layers. (d) LDOS difference Δ defined as LDOS at $\theta = 1/3$ minus that at $\theta = 1/12$. Red color indicates $\Delta > 0$, and blue $\Delta < 0$. The regions $|\Delta| \geq 10^{-4}$ are drawn. Fine structures near the core regions are ignored.

is largely due to a decrease in the Pd LDOS. To study this point further, the partial density of states[21] projected onto each atom in the unit cell was calculated. Figure 8 reveals that K 4s electrons form a broad band across E_F. This contrasts with the narrow valence band of bcc K (about 2.2 eV) and suggests strong mixing with the Pd 4d states. In addition, the number of 4s electrons increases with an increase in θ: 0.15, 0.19, and 0.22 electron per atom at $\theta = 1/12$,

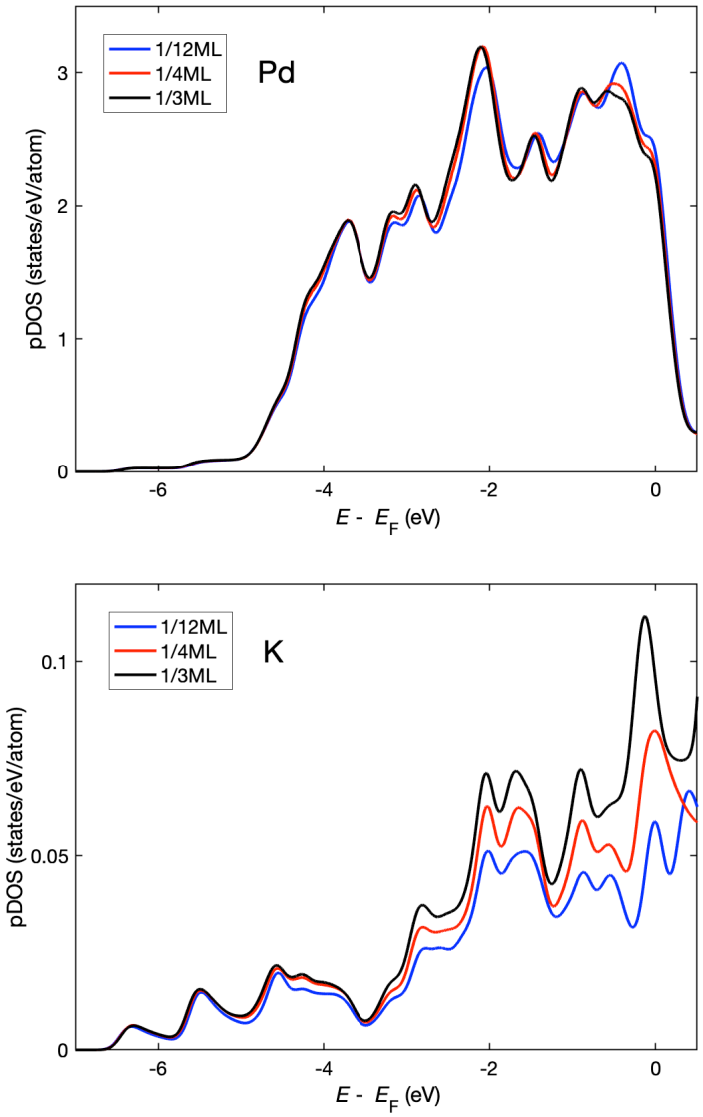

Fig. 8. Partial density of states (pDOS) calculated for the K-row model. The unit of pDOS is the number of states per eV, per atom. For Pd, pDOSs for six first-layer atoms and 12 second-layer atoms in the unit cell are averaged. For K at 1/3 ML, pDOSs for two inequivalent atoms in the unit cell, one at the hollow site and the other at the bridge site (see Fig. 3(c)), are averaged.

1/4, and 1/3, respectively. Therefore, the high K LDOS is attributable to the back donation of electrons from the Pd substrate to the K atoms.

5. Conclusions

The K-induced (1 × 2) reconstruction of Pd(110) was investigated with combined use of scanning tunneling microscopy (STM), work function measurement and ab initio calculations. The surface structure was found to be consistent with the K-row model.[17] The work functions were calculated for the model with various coverages. The calculation is in good agreement

with the experiment. It was found by STM that the K atoms are invisible at coverage of 0.1 monolayer, but appear as bright rows at 0.3 monolayer. The local density of states (LDOS) and partial density of states (pDOS) were also calculated. The LDOS analysis explains why the K atoms are either visible or invisible depending on the coverages. A change in the pDOS with coverage suggests that the back donation of electrons from Pd to K occurs in the course of the K row formation.

Acknowledgments

One of the authors (K.H.) is grateful to Dr. Taizo Sasaki at National Institute for Materials Science for helpful comments and discussion. Part of the ab initio calculation was performed by using the supercomputing resources at Cyberscience Center, Tohoku University.

Appendix

The estimation of K coverage θ was made by using X-ray photoelectron spectroscopy (XPS) and low-energy electron diffraction (LEED). The upper panel of Fig. A·1 shows K2p XPS spectra taken for various K exposures. The spectrum at 0 min is for the (1×2) surface without additional K adsorption. Aluminum K$\alpha_{1,2}$ lines (1487 eV) were used to excite photoelectrons. A broad peak at -271 eV is the Pd3d lines due to Al Kβ_1 satellite (1557 eV). The photoelectrons were collected with use of an angle-integrated cylindrical sector analyzer at normal emission geometry. Variation of the intensity ratio K2p/Pd3d with K exposure is plotted in the lower panel of Fig. A·1. The intensity ratio was evaluated without considering the effects of photoelectron diffraction because they are insignificant in our experimental condition.[37] Figure A·1 shows that the intensity ratio increases linearly with the K exposure. The intensity ratio is proportional to θ. Since the desorption of K at 300 K is negligible for coverages in the range $\theta < 0.35$,[38] the K exposure is also proportional to θ.

Next is to find one-to-one correspondence between the exposure and θ. In a LEED study on Na/Ni(110), Gerlach and Rhodin[15] found that the streaks shift toward the (10) spot with an increase in Na coverage. This shift was attributed to the contraction of Na rows grown on the Ni(110) surface. Figure A·2 shows that the shift stops at 10.56 min. At this time, the streaks are located at $g = 0.69 g_{10}$ (g_{10} is the distance between the (00) and (10) spots). These observations indicate that the contraction of K rows stops at 10.56 min, and that their nearest-neighbor distance is $b/0.69 \approx 3b/2$ ($b = \sqrt{2}a/2$). Thus, we set $\theta(10.56\,\text{min}) = 1/3$. Hörnis and Conrad[19] reported that the (1×2) reconstruction occurs at 0.095 ML. Hence, we set $\theta(0\,\text{min}) = 0.095$. From these, the exposure rate is $(0.333 - 0.095)/10.56 \approx 0.023$ ML/min. The uncertainty is about 10%. This comes mainly from the uncertainty in determining a breakpoint in Fig. A·2. Our coverage assignment, 0.095 ML at 0 min and 1/3 ML at 10.56 min, is consistent with the intensity ratio in Fig. A·1.

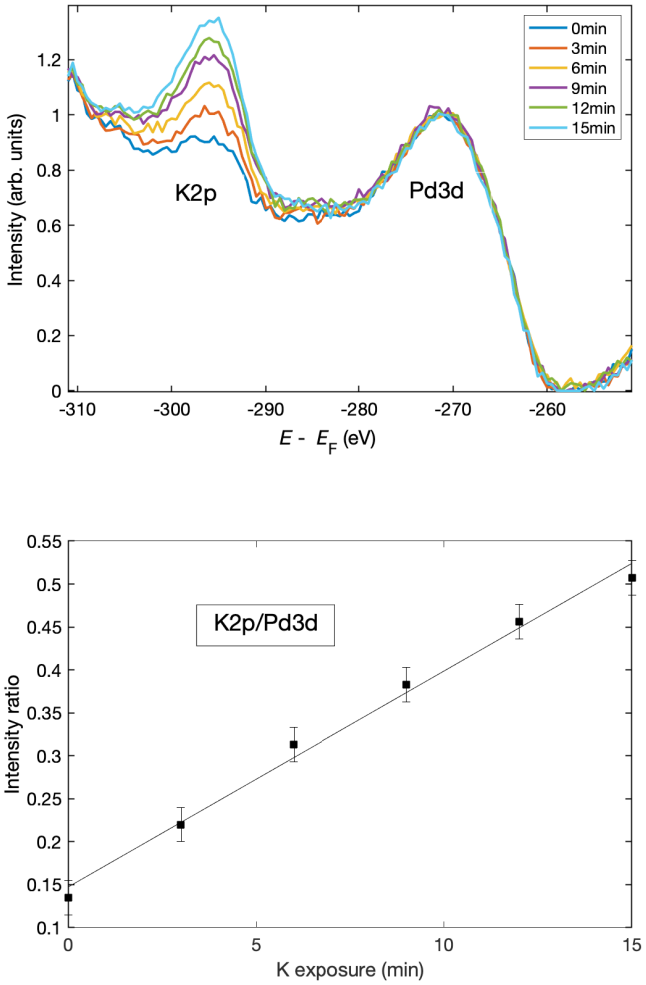

Fig. A·1. The upper panel shows K2p XPS spectra taken for the K/Pd(110)-(1 × 2) surface at various K exposures. Intensity is normalized at -271 eV. The lower panel depicts variation of the intensity ratio K2p/Pd3d with K exposure. A straight line is a least-squares fit to the data.

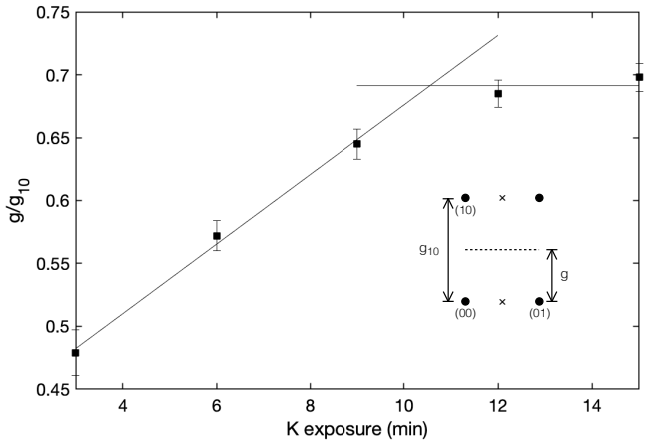

Fig. A·2. Variation of streak position g as a function of K exposure. The inset shows a (1 × 2) LEED pattern, where only the first-order streak is drawn by a dashed line.

References

1) T. Aruga and Y. Murata, Prog. Surf. Sci. **31**, 61 (1989).
2) C.J. Barnes, M.Q. Ding, M. Lindroos, R.D. Diehl, and D.A. King, Surf. Sci. **162**, 59 (1985).
3) C.J. Barnes, M. Lindroos, and D.A. King, Surf. Sci. **201**, 108 (1988).
4) Z.P. Hu, B.C. Pan, W.C. Fan, and A. Ignatiev, Phys. Rev. B**41**, 9692 (1990).
5) R. Schuster, J.V. Barth, G. Ertl, and R.J. Behm, Surf. Sci. **247**, L229 (1991).
6) G. Doyen, D. Drakova, J.V. Barth, R. Schuster, T. Gritsch, R.J. Behm, and G. Ertl, Phys. Rev. B**48**, 1738 (1993).
7) A.F. Carley, P.R. Davies, K.R. Harikumar, R.V. Jones, and M.W. Roberts, J. Phys. Chem. B**108**, 14518 (2004).
8) S. Günther, R. Hoyer, H. Marbach, R. Imbihl, F. Esch, C. Africh, G. Comelli, and M. Kiskinova, J. Chem. Phys. **124**, 014706 (2006).
9) R. Pang, H. Qin, Z. Cai, M. Liu, S. Chen, J. Zhong, and D. Zhong, Surf. Sci. **684**, 18 (2019).
10) M. Copel, W.R. Graham, T. Gustafsson, and S. Yalisove, Solid State Commun. **54**, 695 (1985).
11) J.W.M. Frenken, R.L. Krans, J.F. van der Veen, E. Holub-Krappe, and K. Horn, Phys. Rev. Lett. **59**, 2307 (1987).
12) P. Statiris, P.T. Häberle, and T. Gustafsson, Phys. Rev. B**47**, 16513 (1993).
13) D. Heskett and L.E. Berman, Phys. Rev. B**61**, 8450 (2000).
14) C.-M. Chan, M.A. Van Hove, W.H. Weinberg, and E.D. Williams, Solid State Commun. **30**, 47 (1979).
15) R.L. Gerlach and T.N. Rhodin, Surf. Sci. **10**, 446 (1968).
16) R.L. Gerlach and T.N. Rhodin, Surf. Sci. **17**, 32 (1969).
17) R.J. Behm, D.K. Flynn, K.D. Jamison, G. Ertl, and P.A. Thiel, Phys. Rev. B**36**, 9267 (1987).
18) K.W. Jacobsen and J.K. Nørskov, Phys. Rev. Lett. **60**, 2496 (1988).
19) H. Hörnis and E.H. Conrad, Surf. Sci. **322**, 256 (1995).
20) K. Higashiyama, A. Egami, S. Hosoi, and K. Suzuki, Jpn. J. Appl. Phys. **40**, 6985 (2001).
21) P. Giannozzi, S. Baroni, N. Bonini, M. Calandra, R. Car, C. Cavazzoni et al., J. Phys.: Condens. Matter **21**, 395502 (2009).
22) A. Dal Corso, Phys. Rev. B**86**, 085135 (2012).

23) J.P. Perdew, K. Burke, and M. Ernzerhof, Phys. Rev. Lett. **77**, 3865 (1996).
24) J.P. Perdew, K. Burke, and M. Ernzerhof, Phys. Rev. Lett. **78**, 1396 (1997).
25) H.J. Monkhorst and J.D. Pack, Phys. Rev. B**13**, 5188 (1976).
26) M. Methfessel and A. T. Paxton, Phys. Rev. B**40**, 3616 (1989).
27) N.E. Singh-Miller and N. Marzari, Phys. Rev. B**80**, 235407 (2009).
28) L. Bengtsson, Phys. Rev. B**59**, 12301 (1999).
29) K. Momma and F. Izumi, J. Appl. Cryst. **44**, 1272 (2011).
30) N.D. Lang and W. Kohn, Phys. Rev. B**3**, 1215 (1971).
31) K. Yagi, K. Higashiyama, S. Yamazaki, H. Yanashima, H. Ohnuki, H. Fukutani, and H. Kato, Surf. Sci. **231**, 397 (1990).
32) *CRC Handbook of Chemistry and Physics* (CRC Press, Boca Raton, 2018) 99th ed., p.12-102.
33) C.J. Fall, N. Binggeli, and A. Baldereschi, J. Phys.: Condens. Matter **11**, 2689 (1999).
34) A. Kiejna, J. Peisert, and P. Scharoch, Surf. Sci. **432**, 54 (1999).
35) R. Schuster, J.V. Barth, G. Ertl, and R.J. Behm, Phys. Rev. Lett. **69**, 2547 (1992).
36) J. Tersoff and D.R. Hamann, Phys. Rev. B**31**, 805 (1985).
37) C.S. Fadley, Prog. Surf. Sci. **16**, 275 (1984).
38) S.J. Pratt, D.K. Escott, and D.A. King, Phys. Rev. B**68**, 235406 (2003).